nature photonics

SUPPLEMENTARY INFORMATION
https://doi.org/10.1038/s41566-017-0075-2

In the format provided by the authors and unedited.

Time-reversal symmetry breaking with acoustic pumping of nanophotonic circuits

Donggyu B. Sohn, Seunghwi Kim and Gaurav Bahl *

Mechanical Science and Engineering, University of Illinois at Urbana-Champaign, Urbana, IL, USA. *e-mail: bahl@illinois.edu

Supplementary information: Time-reversal symmetry breaking with acoustic pumping of nanophotonic circuits

Donggyu B Sohn, Seunghwi Kim, and Gaurav Bahl*

Mechanical Science and Engineering, University of Illinois at Urbana-Champaign
Urbana, Illinois 61801, USA
* To whom correspondence should be addressed;
E-mail: bahl@illinois.edu

November 17, 2017

Contents

S1 System Model

S1.1 Dynamics of Traveling Acousto-optical Interaction

Our system consists of two optical modes in a racetrack resonator (quasi-TE_{10} (ω_1, k_1) and quasi-TE_{00} (ω_2, k_2)) that are coupled by means of an acoustic pump (Ω, q) (Fig. S1, S2). The directionality of the acoustic pump is pre-selected via the electromechanical driving stimulus. With respect to this pump, we define "forward" as the direction in which the light and the acoustic pump are co-propagating, and "backward" as the counter-propagating direction.

The interaction Hamiltonian categorized to the forward and backward direction can be expressed as:

$$H_{\text{int}} = \hbar(\beta_f \hat{a}_1 \hat{a}_2^\dagger \hat{b} + \beta_f^* \hat{a}_1^\dagger \hat{a}_2 \hat{b}^\dagger) + \hbar(\beta_b \hat{a}_1 \hat{a}_2^\dagger \hat{b}^\dagger + \beta_b^* \hat{a}_1^\dagger \hat{a}_2 \hat{b}) \tag{S1}$$

where $\beta_f = \beta\,\delta(k_1 - k_2 + q)$ and $\beta_b = \beta\,\delta(-k_1 + k_2 + q)$ are the optomechanical coupling coefficients including the phase matching conditions in the forward and backward directions respectively. Here, $\delta()$ is the Kronecker delta function, $\hat{a}_1^\dagger(\hat{a}_1)$ and $\hat{a}_2^\dagger(\hat{a}_2)$ are the creation (annihilation) operators for the TE_{10} and TE_{00} modes respectively, and $\hat{b}^\dagger(\hat{b})$ is for the acoustic pump [1, 2].

In addition, we include the RF-electromechanically driven acoustic field (s_{RF}). The input acoustic field is defined as $|s_{RF}|^2 = \eta_{\text{a}} P_{RF}/\hbar\Omega$ where P_{RF} is the RF driving power, Ω is the RF driving frequency, η_a is the electromechanical coupling, and Γ is the mechanical loss rate. An externally provided laser (s_{in}) is coupled to the TE_{10} and TE_{00} modes through the external coupling rates κ_{ex1} and κ_{ex2}. As above, the input optical field is defined as $|s_{in}|^2 = P_{in}/\hbar\omega_l$ where P_{in} is the input laser power and ω_l is the frequency of carrier laser. Therefore, the total effective Hamiltonian for the system can be written as [3]:

$$\begin{aligned} H_{\text{eff}} = {} & \hbar\omega_1 \hat{a}_1^\dagger \hat{a}_1 + \hbar\omega_2 \hat{a}_2^\dagger \hat{a}_2 + \hbar\omega_m \hat{b}^\dagger \hat{b} \\ & + \hbar\,(\beta_f \hat{a}_1 \hat{a}_2^\dagger \hat{b} + \beta_f^* \hat{a}_1^\dagger \hat{a}_2 \hat{b}^\dagger) + \hbar\,(\beta_b \hat{a}_1 \hat{a}_2^\dagger \hat{b}^\dagger + \beta_b^* \hat{a}_1^\dagger \hat{a}_2 \hat{b}) \\ & + i\hbar\sqrt{\kappa_{ex1}}\,(\hat{a}_1^\dagger s_{in} e^{-i\omega_l t} - \hat{a}_1 s_{in}^* e^{i\omega_l t}) + i\hbar\sqrt{\kappa_{ex2}}\,(\hat{a}_2^\dagger s_{in} e^{-i\omega_l t} - \hat{a}_2 s_{in}^* e^{i\omega_l t}) \\ & + i\hbar\sqrt{\Gamma}\,(\hat{b}^\dagger s_{RF} e^{-i\Omega t} - \hat{b} s_{RF}^* e^{i\Omega t}) \end{aligned} \tag{S2}$$

Working in a frame rotating with the RF driving frequency (Ω), we write the equations of motion for the mechanical and optical modes by means of Heisenberg-Langevin equation:

$$\dot{\hat{b}} = -\, i(\omega_m - \Omega)\hat{b} - \frac{\Gamma}{2}\hat{b} - i\beta_f^* \hat{a}_1^\dagger \hat{a}_2 e^{i\Omega t} - i\beta_b \hat{a}_1 \hat{a}_2^\dagger e^{i\Omega t} + \sqrt{\Gamma}\, s_{RF} \tag{S3a}$$

$$\dot{\hat{a}}_1 = -\, i\omega_1 \hat{a}_1 - \frac{\kappa_1}{2}\hat{a}_1 - i\beta_f^* \hat{a}_2 \hat{b}^\dagger e^{i\Omega t} - i\beta_b^* \hat{a}_2 \hat{b} e^{-i\Omega t} + \sqrt{\kappa_{ex1}}\, s_{in} e^{-i\omega_l t} \tag{S3b}$$

$$\dot{\hat{a}}_2 = -\, i\omega_2 \hat{a}_2 - \frac{\kappa_2}{2}\hat{a}_2 - i\beta_f \hat{a}_1 \hat{b} e^{-i\Omega t} - i\beta_b \hat{a}_1 \hat{b}^\dagger e^{i\Omega t} + \sqrt{\kappa_{ex2}}\, s_{in} e^{-i\omega_l t} \tag{S3c}$$

where κ_1 (κ_2) are the optical loss rates of the TE_{10} (TE_{00}) modes.

We will now distill the above general equations for the two specific cases in which light enters from the forward and backward directions.

S1.2 Scattering Process in the Forward Direction (Co-propagating Direction)

We treat the equations of motion in Eq. (S3) classically by making substitutions as follows: $\hat{a}_1, (\hat{a}_2) \rightarrow a_1$ (a_2) and $\hat{b} \rightarrow u$. Thus a_1 and a_2 are the amplitudes of the TE_{10} and TE_{00} intracavity fields respectively and u is the steady state amplitude of the acoustic field under the non-depleted RF pump approximation. We consider the situation illustrated in Fig. S1, where phase matching only occurs for forward propagating light ($k_1 - k_2 + q = 0$). Here, the non-phase matched terms can be neglected, i.e. the term with β_b in Eq. S3. We can also drop $\delta()$ in the forward intermodal coupling coefficient and simply use β as the optomechanical coupling rate. The TE_{10} mode can only convert into the TE_{00} mode through anti-Stokes scattering. Similarly, the TE_{00} mode can only convert into the TE_{10} mode through Stokes scattering. Thus, we can rewrite Eq. S3 as:

$$\dot{a_1} = -\frac{\kappa_1}{2}a_1 - i\omega_1 a_1 - i\beta^* u^* a_2 e^{i\Omega t} + \sqrt{\kappa_{ex1}}\, s_{in} e^{-i\omega_l t} \tag{S4a}$$

$$\dot{a_2} = -\frac{\kappa_2}{2}a_2 - i\omega_2 a_2 - i\beta u a_1 e^{-i\Omega t} + \sqrt{\kappa_{ex2}}\, s_{in} e^{-i\omega_l t} \tag{S4b}$$

The mode amplitudes a_1 and a_2 can be now expressed through Fourier decomposition of the sidebands created by the intermodal scattering:

$$a_1 = \sum_{n=-\infty}^{\infty} a_{1,n} e^{-i(\omega_l + n\Omega)t} \;=\; a_{1,-1} e^{-i(\omega_l - \Omega)t} + a_{1,0} e^{-i\omega_l t} \tag{S5a}$$

$$a_2 = \sum_{n=-\infty}^{\infty} a_{2,n} e^{-i(\omega_l + n\Omega)t} \;=\; a_{2,0} e^{-i\omega_l t} + a_{2,+1} e^{-i(\omega_l + \Omega)t} \tag{S5b}$$

where n indicates the sideband order. Here, we adopted the following convention: $a_{i,0}$ is the intracavity field at the carrier frequency, while $a_{i,-1}$ ($a_{i,+1}$) are the intracavity fields at the Stokes (anti-Stokes) shifted frequency for the ith order mode. Thus, $a_{1,0}$ ($a_{2,0}$) are the intracavity field amplitude for TE_{10} (TE_{00}) mode at the carrier frequency i.e. the frequency of the source laser. $a_{1,-1}$ is the Stokes sideband amplitude for the TE_{10} mode. $a_{2,+1}$ is the anti-Stokes sideband amplitude for the TE_{00} mode. The remaining sidebands are suppressed due to the phase matching condition, i.e. absence of suitable optical modes.

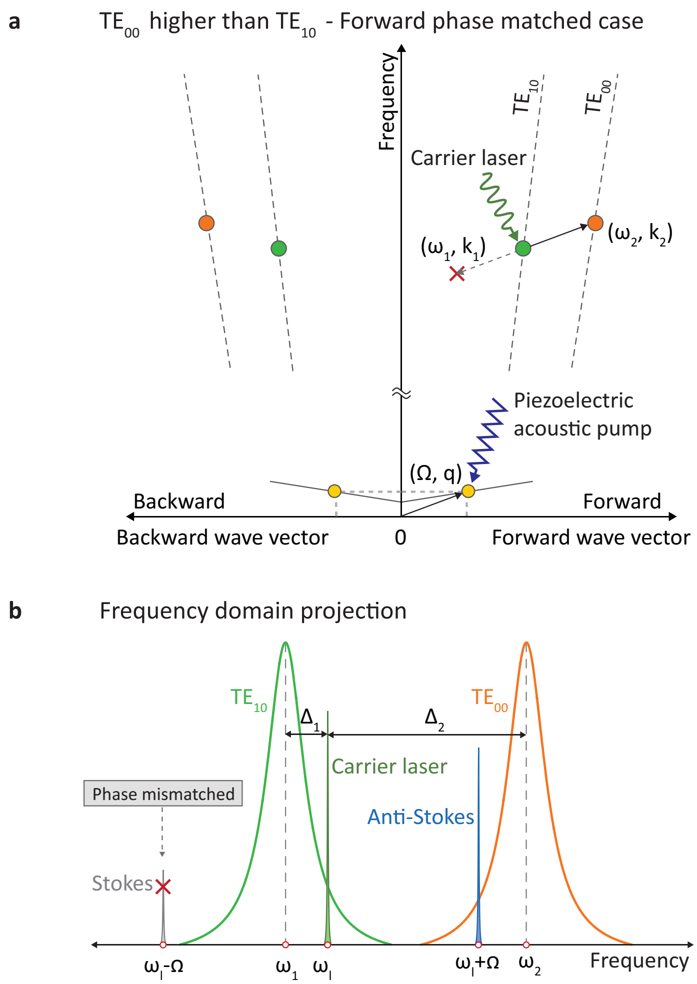

Figure S1: (a) Intermodal scattering illustrated in frequency-momentum space. In the case where the carrier laser is presented to the TE_{10} mode in the forward direction, the anti-Stokes sideband is resonantly enhanced by the TE_{00} resonance mode. The Stokes sideband is suppressed since there is no optical mode available. (b) The intermodal scattering process illustrated in frequency domain. Due to the energy-momentum phase matching condition only the anti-Stokes sideband appears, which is located at the frequency $\omega_l + \Omega$.

The intracavity field amplitudes $a_{1,0}$, $a_{2,0}$, $a_{1,-1}$ and $a_{2,+1}$ are obtained by substituting Eq. (S5) to Eq. (S4).

$$a_{1,0} = \frac{\sqrt{\kappa_{ex1}}\, s_{in} - i\beta^* u^* a_{2,+1}}{\kappa_1/2 - i\Delta_1} \quad \text{and} \quad a_{2,0} = \frac{\sqrt{\kappa_{ex2}}\, s_{in} - i\beta u a_{1,-1}}{\kappa_2/2 - i\Delta_2}$$
$$a_{1,-1} = \frac{-i\beta^* u^* a_{2,0}}{\kappa_1/2 - i(\Delta_1 - \Omega)} \quad \text{and} \quad a_{2,+1} = \frac{-i\beta u a_{1,0}}{\kappa_2/2 - i(\Delta_2 + \Omega)} \tag{S6}$$

where the optical detunings are $\Delta_1 = \omega_l - \omega_1$ and $\Delta_2 = \omega_l - \omega_2$.

In the solutions for the carrier frequency components ($a_{1,0}$ and $a_{2,0}$), the first term in the numerator is the input field coupled from the optical waveguide and the second term is the field scattered back from the corresponding sideband. The sideband intracavity fields can be finally expressed in terms of the input laser (s_{in}) as follows:

$$a_{1,0} = \frac{\sqrt{\kappa_{ex1}}\,(\kappa_2/2 - i(\Delta_2 + \Omega))}{(\kappa_2/2 - i(\Delta_2 + \Omega))\,(\kappa_1/2 - i\Delta_1) + |\beta|^2|u|^2} s_{in}, \tag{S7a}$$
$$a_{2,0} = \frac{\sqrt{\kappa_{ex2}}(\kappa_1/2 - i(\Delta_1 - \Omega))}{(\kappa_1/2 - i(\Delta_1 - \Omega))(\kappa_2/2 - i\Delta_2) + |\beta|^2|u|^2} s_{in}, \tag{S7b}$$
$$a_{1,-1} = \frac{-i\beta^* u^* \sqrt{\kappa_{ex2}}}{(\kappa_1/2 - i(\Delta_1 - \Omega))(\kappa_2/2 - i\Delta_2) + |\beta|^2|u|^2} s_{in}, \tag{S7c}$$
$$a_{2,+1} = \frac{-i\beta u \sqrt{\kappa_{ex1}}}{(\kappa_2/2 - i(\Delta_2 + \Omega))(\kappa_1/2 - i\Delta_1) + |\beta|^2|u|^2} s_{in}. \tag{S7d}$$

When the optomechanical coupling rate is much smaller than the optical loss rate ($|\beta||u| << \sqrt{\kappa_1\kappa_2}/2$), e.g. for small acoustic drive (u), Eq. S6 can be simplified to:

$$a_{1,0} = \frac{\sqrt{\kappa_{ex1}}}{\kappa_1/2 - i\Delta_1} s_{in}, \tag{S8a}$$
$$a_{2,0} = \frac{\sqrt{\kappa_{ex2}}}{\kappa_2/2 - i\Delta_2} s_{in}, \tag{S8b}$$
$$a_{1,-1} = \frac{-i\beta^* u^* \sqrt{\kappa_{ex2}}}{(\kappa_1/2 - i(\Delta_1 - \Omega))(\kappa_2/2 - i\Delta_2)} s_{in}, \tag{S8c}$$
$$a_{2,+1} = \frac{-i\beta u \sqrt{\kappa_{ex1}}}{(\kappa_2/2 - i(\Delta_2 + \Omega))(\kappa_1/2 - i\Delta_1)} s_{in} \tag{S8d}$$

By means of input output theorem, we obtain the expression for the output spectrum (s_{out}) from the waveguide containing carrier ($s_{out,0}$), Stokes ($s_{out,-1}$), and anti-Stokes ($s_{out,+1}$) frequency components:

$$s_{out} = s_{out,0} + s_{out,+1} e^{-i\Omega t} + s_{out,-1} e^{i\Omega t} \tag{S9}$$

where

$$
\begin{aligned}
s_{out,0} &= s_{in} - \sqrt{\kappa_{ex1}}\, a_{1,0} - \sqrt{\kappa_{ex2}}\, a_{2,0} && \text{(S10a)}\\
s_{out,-1} &= -\sqrt{\kappa_{ex1}}\, a_{1,-1} && \text{(S10b)}\\
s_{out,+1} &= -\sqrt{\kappa_{ex2}}\, a_{2,+1} && \text{(S10c)}
\end{aligned}
$$

These equations represent ideal interband scattering when the light enters in the forward direction.

S1.3 Scattering Process in the Backward Direction (Counter-propagating Direction)

Let us now consider the case shown in Fig. S2 where the light propagating direction is in the backward direction. Due to the backward phase matching condition ($-k_1 + k_2 + q = 0$), as opposed to the scattering in the forward direction, the TE_{10} (TE_{00}) modes can only convert into the TE_{00} (TE_{10}) modes through Stokes (anti-Stokes) scattering. When the resonance frequency of the TE_{10} mode is higher than the TE_{00} mode, the phase matching condition is satisfied in the backward direction. Thus, in this case, the equations of motion in Eq. S3 are simplified to:

$$
\begin{aligned}
\dot{a_1} &= -\frac{\kappa_1}{2}a_1 - i\omega_1 a_1 - i\beta^* u a_2 e^{-i\Omega t} + \sqrt{\kappa_{ex1}}\, s_{in} e^{-i\omega_l t} && \text{(S11a)}\\
\dot{a_2} &= -\frac{\kappa_2}{2}a_2 - i\omega_2 a_2 - i\beta u^* a_1 e^{i\Omega t} + \sqrt{\kappa_{ex2}}\, s_{in} e^{-i\omega_l t} && \text{(S11b)}
\end{aligned}
$$

The composited amplitudes a_1 and a_2 can be written as:

$$
\begin{aligned}
a_1 =& a_{1,0} e^{-i\omega_l t} + a_{1,+1} e^{-i(\omega_l+\Omega)t} && \text{(S12a)}\\
a_2 =& a_{2,-1} e^{-i(\omega_l-\Omega)t} + a_{2,-1} e^{-i\omega_l t} && \text{(S12b)}
\end{aligned}
$$

where $a_{1,+1}$ is the anti-Stokes sideband amplitude in the TE_{10} mode, and $a_{2,-1}$ is the Stokes sideband amplitude in the TE_{00} mode.

$$
\begin{aligned}
a_{1,0} &= \frac{\sqrt{\kappa_{ex1}}\, s_{in} - i\beta^* u a_{2,-1}}{\kappa_1/2 - i\Delta_1} \quad \text{and} \quad a_{2,0} = \frac{\sqrt{\kappa_{ex2}}\, s_{in} - i\beta u^* a_{1,+1}}{\kappa_2/2 - i\Delta_2}\\
a_{1,+1} &= \frac{-i\beta^* u a_{2,0}}{\kappa_1/2 - i(\Delta_1+\Omega)} \quad \text{and} \quad a_{2,-1} = \frac{-i\beta u^* a_{1,0}}{\kappa_2/2 - i(\Delta_2-\Omega)} && \text{(S13)}
\end{aligned}
$$

The sideband intracavity fields can be expressed in terms of the input laser (s_{in}) as follows:

$$
a_{1,0} = \frac{\sqrt{\kappa_{ex1}}\,(\kappa_2/2 - i(\Delta_2-\Omega))}{(\kappa_2/2 - i(\Delta_2-\Omega))\,(\kappa_1/2 - i\Delta_1) + |\beta|^2|u|^2} s_{in}, \qquad \text{(S14a)}
$$

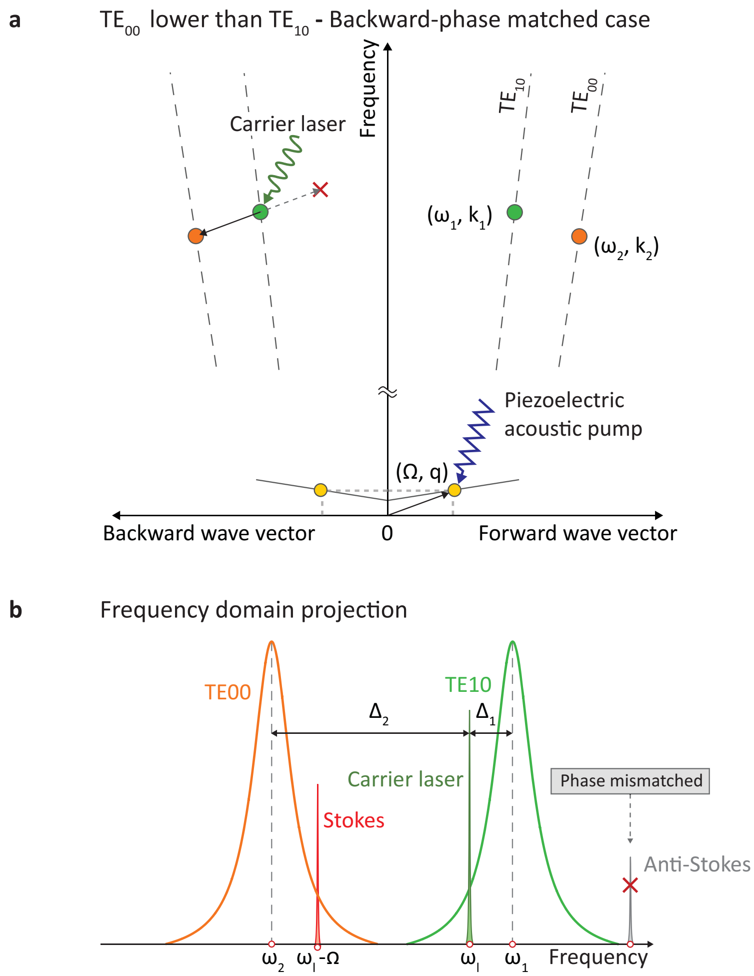

Figure S2: (a) Intermodal scattering illustrated in frequency-momentum space. In the case where the carrier laser is presented to the TE_{10} mode in the backward direction, the Stokes sideband is resonantly enhanced by the TE_{10} mode. The anti-Stokes sideband is suppressed since there is no optical mode that allows scattering. (b) The intermodal scattering illustrated in frequency domain. Due to the phase matching condition only the Stokes sideband appears, which is located at the frequency $\omega_l - \Omega$.

$$a_{2,0} = \frac{\sqrt{\kappa_{ex2}}(\kappa_1/2 - i(\Delta_1 + \Omega))}{(\kappa_1/2 - i(\Delta_1 + \Omega))(\kappa_2/2 - i\Delta_2) + |\beta|^2|u|^2} s_{in}, \tag{S14b}$$

$$a_{1,+1} = \frac{-i\beta^* u\sqrt{\kappa_{ex2}}}{(\kappa_1/2 - i(\Delta_1 + \Omega))(\kappa_2/2 - i\Delta_2) + |\beta|^2|u|^2} s_{in}, \tag{S14c}$$

$$a_{2,-1} = \frac{-i\beta u^* \sqrt{\kappa_{ex1}}}{(\kappa_2/2 - i(\Delta_2 - \Omega))(\kappa_1/2 - i\Delta_1) + |\beta|^2|u|^2} s_{in}. \tag{S14d}$$

When the optomechanical coupling rate is much smaller than the optical loss rate ($|\beta||u| << \sqrt{\kappa_1\kappa_2}/2$), e.g. for small acoustic drive (u), Eq. S13 can be simplified to:

$$a_{1,0} = \frac{\sqrt{\kappa_{ex1}}}{\kappa_1/2 - i\Delta_1} s_{in}, \tag{S15a}$$

$$a_{2,0} = \frac{\sqrt{\kappa_{ex2}}}{\kappa_2/2 - i\Delta_2} s_{in}, \tag{S15b}$$

$$a_{1,+1} = \frac{-i\beta^* u\sqrt{\kappa_{ex2}}}{(\kappa_1/2 - i(\Delta_1 + \Omega))(\kappa_2/2 - i\Delta_2)} s_{in}, \tag{S15c}$$

$$a_{2,-1} = \frac{-i\beta u^* \sqrt{\kappa_{ex1}}}{(\kappa_2/2 - i(\Delta_2 - \Omega))(\kappa_1/2 - i\Delta_1)} s_{in} \tag{S15d}$$

Similar to the output from the previous section, the output spectrum (s_{out}) from the waveguide contains the carrier ($s_{out,0}$), Stokes ($s_{out,-1}$), and anti-Stokes ($s_{out,+1}$) frequency components:

$$s_{out} = s_{out,0} + s_{out,+1}\, e^{-i\Omega t} + s_{out,-1}\, e^{i\Omega t} \tag{S16}$$

where

$$s_{out,0} = s_{in} - \sqrt{\kappa_{ex1}}\, a_{1,0} - \sqrt{\kappa_{ex2}}\, a_{2,0} \tag{S17a}$$

$$s_{out,-1} = -\sqrt{\kappa_{ex2}}\, a_{2,-1} \tag{S17b}$$

$$s_{out,+1} = -\sqrt{\kappa_{ex1}}\, a_{1,+1} \tag{S17c}$$

These equations represent ideal interband scattering when the light enters in the backward direction.

S1.4 Residual Intra-modal Light Scattering

Our experimental measurements exhibit residual light scattering signatures that are consistent with intra-modal light scattering even in cases without correct inter-modal phase matching. This additional scattering can arise due to acousto-optical misalignment in the experimental device and due to waveguide curvature. Here, we incorporate intramodal scattering into the theoretical model [4] by introducing two additional scattering terms in the equations of motion for the optical modes (we show here for the forward case of Eqns. S4):

$$\dot{a_1} = -\frac{\kappa_1}{2}a_1 - i\left(\omega_1 + g_1 u\cos(\Omega t)\right)a_1 - i\beta^* u^* a_2 e^{i\Omega t} + \sqrt{\kappa_{ex1}}\, s_{in} e^{-i\omega_l t} \tag{S18a}$$

$$\dot{a_2} = -\frac{\kappa_2}{2}a_2 - i\left(\omega_2 + g_2 u\cos(\Omega t)\right)a_2 - i\beta u a_1 e^{-i\Omega t} + \sqrt{\kappa_{ex2}}\, s_{in} e^{-i\omega_l t}\ . \tag{S18b}$$

Here g_1 and g_2 are the newly introduced intramodal optomechanical coupling coefficients for the TE_{10} and TE_{00} modes respectively. We consider the case where modulation amplitude is relatively small so that the sidebands from intramodal and intermodal scattering can be independently calculated. As before, we can perform a Fourier decomposition of the optical sidebands a_1 and a_2 with a particular focus on the intramodal modulation terms (ignoring intermodal scattering terms):

$$a_1 = \sum_{n=-\infty}^{\infty} a_{1,n}^{(r)} e^{-i(\omega_l + n\Omega)t} \tag{S19}$$

$$a_2 = \sum_{n=-\infty}^{\infty} a_{2,n}^{(r)} e^{-i(\omega_l + n\Omega)t} \tag{S20}$$

Here, we use the superscript (r) to indicate terms arising from the residual intramodal scattering.

In the resolved sideband regime ($\Omega > \kappa_1/2$ and $\kappa_2/2$) higher order sidebands ($n \geq 1$) can generally be neglected. Using the same analysis as before, the intracavity fields at the Stokes ($a_{i,-1}^{(r)}$) and anti-Stokes ($a_{i,+1}^{(r)}$) sidebands resulting from residual scattering only can be calculated as:

$$a_{1,\pm1}^{(r)} = \frac{-ig_1 u\sqrt{\kappa_{ex1}}}{(\kappa_1/2 - i(\Delta_1 \pm \Omega))(\kappa_1/2 - i\Delta_1)} s_{in}, \tag{S21a}$$

$$a_{2,\pm1}^{(r)} = \frac{-ig_2 u\sqrt{\kappa_{ex2}}}{(\kappa_2/2 - i(\Delta_2 \pm \Omega))(\kappa_2/2 - i\Delta_2)} s_{in} \tag{S21b}$$

Finally, the output spectrum measured in the waveguide incorportating both intramodal and intermodal scattering can be calculated. When the light enters in the forward direction, the transmission ($s_{out,+1}$), Stokes ($s_{out,-1}$), and anti-Stokes ($s_{out,+1}$) terms in the waveguide are expressed as:

$$s_{out,0} = s_{in} - \sqrt{\kappa_{ex1}}\, a_{1,0} - \sqrt{\kappa_{ex2}}\, a_{2,0} \tag{S22a}$$

$$s_{out,-1} = -\sqrt{\kappa_{ex1}}\left(a_{1,-1} + a_{1,-1}^{(r)}\right) - \sqrt{\kappa_{ex2}}\, a_{2,-1}^{(r)} \tag{S22b}$$

$$s_{out,+1} = -\sqrt{\kappa_{ex1}}\, a_{1,+1}^{(r)} - \sqrt{\kappa_{ex2}}\left(a_{2,+1} + a_{2,+1}^{(r)}\right) \tag{S22c}$$

Similarly, when the light enters in the backward direction, the output spectrum from the waveguide can be expressed using:

$$s_{out,0} = s_{in} - \sqrt{\kappa_{ex1}}\, a_{1,0} - \sqrt{\kappa_{ex2}}\, a_{2,0} \tag{S23a}$$

$$s_{out,-1} = -\sqrt{\kappa_{ex1}}\, a^{(r)}_{1,-1} - \sqrt{\kappa_{ex2}} \left(a_{2,-1} + a^{(r)}_{2,-1} \right) \tag{S23b}$$

$$s_{out,+1} = -\sqrt{\kappa_{ex1}} \left(a_{1,+1} + a^{(r)}_{1,+1} \right) - \sqrt{\kappa_{ex2}}\, a^{(r)}_{2,+1} \tag{S23c}$$

The above expressions are used to plot the fits of experimental data to theory presented in the manuscript.

S2 Measurement of Optical Spectra

In order to measure the amplitude of the Stokes and anti-Stokes sidebands separately, we utilize optical heterodyne detection with assistance of an acousto-optic frequency shifter (AOFS). The detailed experimental setup is shown in Fig.S3.

Considering the frequency up-shifted reference signal ($s_r e^{-i\Omega_r t}$) generated from the

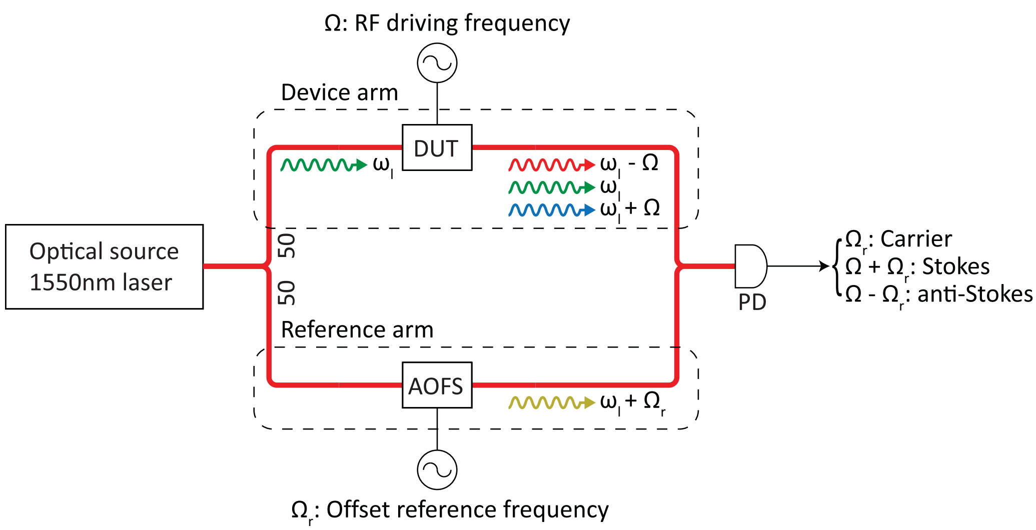

Figure S3: Measurement setup utilizing optical heterodyne detection. The light from the optical source is split into the reference arm and the device arm. The frequency of the light in the reference arm is shifted by the AOFS by predetermined offset Ω_r. The beat notes of the frequency shifted reference with the carrier, Stokes, and anti-Stokes from the device under test (DUT) are measured by the photodetector and have frequency components Ω_r, $\Omega + \Omega_r$, and $\Omega - \Omega_r$ respectively.

AOFS in the reference arm, the optical output spectrum at the photodector can be expressed as:

$$s_{out} = s_{out,0} + s_{out,+1}\, e^{-i\Omega t} + s_{out,-1}\, e^{i\Omega t} + s_r\, e^{-i\Omega_r t} \tag{S24}$$

The resulting electronic signals from the photodetector are beat notes of the optical reference signal with the carrier, Stokes, and anti-Stokes signals, and occur at Ω_r, $\Omega + \Omega_r$, and $\Omega - \Omega_r$ respectively. The powers of each frequency component can be independently measured using an electronic spectrum analyzer. Solving Eq. (S24) for each frequency component while considering the photodetector gain, the RF outputs are expressed as:

$$\begin{aligned} P_{C,\Omega_r} &= g_{pd}|s_r|^2|s_{out,0}|^2 \\ P_{S,\Omega+\Omega_r} &= g_{pd}|s_r|^2|s_{out,-1}|^2 \\ P_{AS,\Omega-\Omega_r} &= g_{pd}|s_r|^2|s_{out,+1}|^2 \end{aligned} \tag{S25}$$

where P_{C,Ω_r}, $P_{S,\Omega+\Omega_r}$, and $P_{AS,\Omega-\Omega_r}$ are the carrier, Stokes, and anti-Stokes RF power outputs from the photodetector, respectively. Here, g_{pd} is the lumped proportionality constant including photodetector gain.

Since the acousto-optic scattering process is linearly proportional to the input light power, the optical power from the output waveguide should normalize to the input light power:

$$P_{in} = g_{pd}|s_r|^2|s_{in}|^2$$

Dividing the measured power by the input power, the normalized power coefficients are given by:

$$\begin{aligned} \bar{P}_{C,\Omega_r} &= \left|\frac{s_{out,0}}{s_{in}}\right|^2 \\ \bar{P}_{S,\Omega+\Omega_r} &= \left|\frac{s_{out,-1}}{s_{in}}\right|^2 \\ \bar{P}_{AS,\Omega-\Omega_r} &= \left|\frac{s_{out,+1}}{s_{in}}\right|^2 \end{aligned} \tag{S26}$$

We use these coefficients to quantify the performance of this mode converting modulator.

S3 Theoretical Limit of Sideband Amplitude

We now wish to theoretically quantify the maximum sideband amplitude achievable in this system. Let us recall the intracavity Stokes sideband field amplitude (Eq. S10b) for the TE_{10} mode. Here, we introduce the phonon enhanced optomechanical coupling rate $G_{ph} = \beta u$. The Stokes sideband from the waveguide $s_{out,-1}$ is:

$$s_{out,-1} = \sqrt{\kappa_{ex1}} \left(\frac{-iG_{ph}^* \sqrt{\kappa_{ex2}}}{(\kappa_1/2 - i(\Delta_1 - \Omega))(\kappa_2/2 - i\Delta_2) + |G_{ph}|^2} \right) s_{in} \tag{S27}$$

From the above equation, we can see that the sideband amplitude is maximized when the frequency matching between the modes is perfect ($\omega_1 - \omega_2 + \Omega = 0$) and the carrier is located on the resonance of the TE_{00} mode. As a result, the imaginary parts in the denominator vanish and the equation can be simplified to:

$$s_{out,-1} = \frac{-iG_{ph}^* \sqrt{\kappa_{ex1}\kappa_{ex2}}}{\kappa_1\kappa_2/4 + |G_{ph}|^2} s_{in} \tag{S28}$$

To investigate the thoeretical limit of sideband amplitude with respect to phonon-enhanced optomechanical coupling G_{ph}, we calculate the maximum point where G_{ph} satisfies $\frac{\partial s_{out,-1}}{\partial G_{ph}} = 0$, which is:

$$G_{ph} = \frac{\sqrt{\kappa_1\kappa_2}}{2} \tag{S29}$$

At this pump level, the calculated maximum sideband field amplitude becomes:

$$s_{out,-1}|_{max} = \sqrt{\frac{\kappa_{ex1}\kappa_{ex2}}{\kappa_1\kappa_2}} s_{in} \tag{S30}$$

This is the point where the photon energy exchange between the two optical modes a_1 and a_2 is in equilibrium. From the equation, we can see that if there is no intrinsic photon loss in the resonator, which means that the external couplings are only photon loss mechanism ($\kappa_{ex1} = \kappa_1, \kappa_{ex2} = \kappa_2$), 100% of light can be transfered to the sideband. In case where both optical modes are critically coupled to the waveguide ($\kappa_{ex1} = \kappa_1/2, \kappa_{ex2} = \kappa_2/2$), the maximum sideband amplitude is 25% of carrier power (50% of carrier field). The rest of power is dissipated in the resonator. If the acoustic pump increases beyond this point, the optical modes split, i.e the system enters the strong coupling regime (see Supplement §S5).

S4 Optomechanical Coupling Coefficient

In order to quantify the intermodal optomechanical coupling coefficient (β) from the experimental data, we employ the model used in [4]. From the fitting of experimental data shown in Fig.5a (main manuscript), we obtain $G_{ph} = |\beta||u| = 0.073$ GHz when 0 dBm of RF input power is supplied. Since, $|\beta|$ and $|u|$ cannot be independently determined from

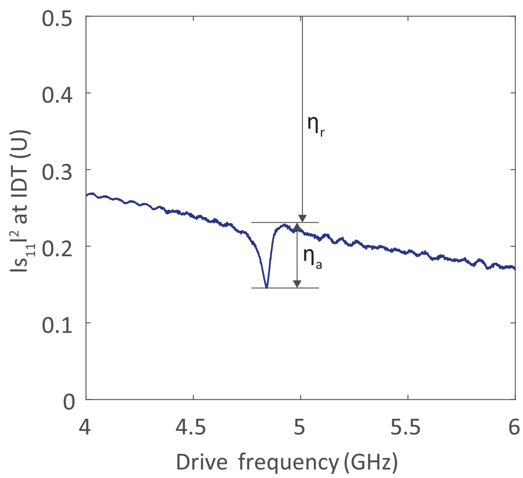

Figure S4: Reflection (s_{11}) measurement at IDT using a calibrated vector network analyzer (VNA). The S_0 Lamb acoustic wave is efficiently actuated at 4.82 GHz leading to a reduction in the s_{11} parameter (reflection). η_a is the efficiency of conversion of electrical power to acoustic power. η_r is the power loss at the IDT through parasitic capacitance.

our fitting model, the displacement u associated with the acoustic wave is estimated with the assistance of finite element simulation (COMSOL). The displacement associated with the acoustic pump for a given RF power is calculated using:

$$u = \sqrt{\frac{2\pi\eta_a P_{RF}}{\gamma W \Omega}} \tag{S31}$$

where W is the IDT aperture, and γ is the proportionality factor relating u^2 and acoustic energy $\gamma = \frac{1}{Wu^2}\int_{x,y,z=0}^{x,y,z=\Lambda,W,\infty} U(x,y,z)dxdydz$, Λ is the wavelength of acoustic pump, and U is the total mechanical energy density of mechanical mode.

The RF power transferred to the acoustic pump power is calculated using the s_{11} parameter measurement with an electronic VNA. As shown in Fig. S4, $\eta_a =$ 3.9%, implying that 3.9% of the RF power is transferred to the acoustic power. γ of the S_0 acoustic mode generated by the IDTs is calculated using FEM simulation ($=2.55 \times 10^{11} J/m^3$). From the fitting of Fig. 5a, the calculated β is found to be 1.64 GHz/nm.

The calculated optomechanical coupling coefficient β quantifies how efficiently the acoustic wave can couple the two optical modes. Note that the estimated displacement u in the above model is the acoustic response of the IDT, which is not the actual amplitude of the acoustic pump traveling in the waveguide. This is a limitation since there exist multiple sources of loss such as intrinsic acoustic loss of the material or reflections from the waveguide ridge, that do not permit a better estimate.

S5 Producing an Optical Isolator

An optical isolator that blocks light in one direction but allows light transmission in the other direction is a canonical example of a non-reciprocal device (Fig. S5). Here, we propose a theoretical model to build a magnetless optical isolator by simply changing few design parameters of our device.

Let us examine at the transmission spectrum of the TE_{10} mode in the forward phase matched case (Eq. S16). We assume that the mechanical driving frequency and the frequency separation between the two optical modes are the same ($\omega_2 - \omega_1 = \Omega$) so that the intermodal scattering can most efficiently take place. We also assume that the sideband is in the fully resolved regime ($\Omega >> \kappa_1/2$ and $\kappa_2/2$). The power transmission from the waveguide in the forward direction can be now expressed as:

$$|s_{out}|^2 = |s_{in} - \sqrt{\kappa_{ex1}} a_{1,0} + \sqrt{\kappa_{ex2}} a_{2,+1} e^{-i\Omega t}|^2 \tag{S32}$$

We note that $a_{2,0}$ and $a_{1,-1}$ terms approach zero when $\Delta_1 << \omega_2 - \omega_1$. Here, we make the TE_{10} mode critically coupled to the waveguide ($\kappa_{ex1} = \kappa_1/2 = 1$ GHz) so that there is no

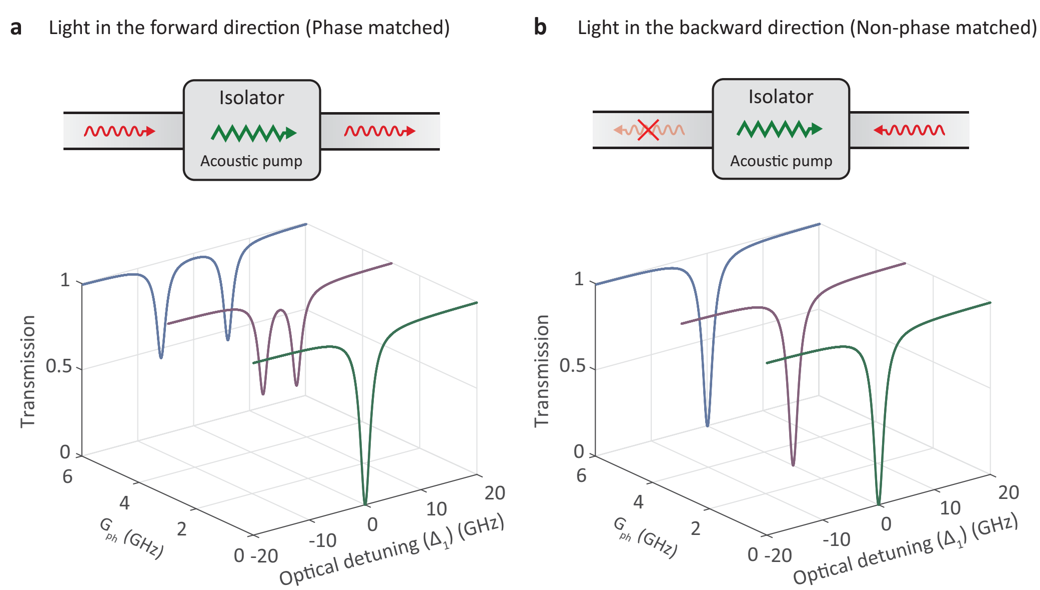

Figure S5: Conceptual schematic of optical isolator and 3D plot of light transmission spectrum respect to optomechanical coupling rate (G_{ph}) and TE_{10} detuning (Δ_1). (a) In the forward direction (phase matched direction), the optical mode is split and the transmission approaches 100 % on resonance ($\Delta_1 = 0$) for large optomechanical coupling. (b) In the backward direction (non-phase matched direction) the optical mode shape remains the same so that light is absorbed by the resonator.

transmission through the waveguide. We also assume that the optical loss rate of TE_{00} (κ_2) is 1 GHz. Using this equation, we plot the forward and backward transmission spectrum (Fig. S5) with respect to the optical detuning of the laser from the TE_{10} mode (Δ_1). Without optomechanical coupling ($G_{ph} = 0$), the backward and forward transmissions exhibit identical Lorentzian shape transmission absorbing all the light on the resonance of the TE_{10} mode ($\Delta_1 = 0$) as shown in Fig. S5. When the optomechanical coupling enters the strong coupling regime ($G_{ph} > \sqrt{\kappa_1\kappa_2}/2$), the TE_{10} resonance mode begins to split (Fig. S5a). With sufficient acoustic power, the system becomes completely transparent at zero detuning only in the forward direction. In the backward direction, where the phase matching condition is not satisfied, the TE_{10} resonance mode remains the same (Fig. S5b) so that all the light is absorbed by the resonator.

S6 Producing an Acousto-optic Frequency Shifter (AOFS)

For an ideal AOFS, we desire carrier transmission to be attenuated so that the output of the device is only the frequency shifted light (Fig. S6a). In this section, we theoretically provide an example of a chip-scale acousto-optic frequency shifter (AOFS) using our device.

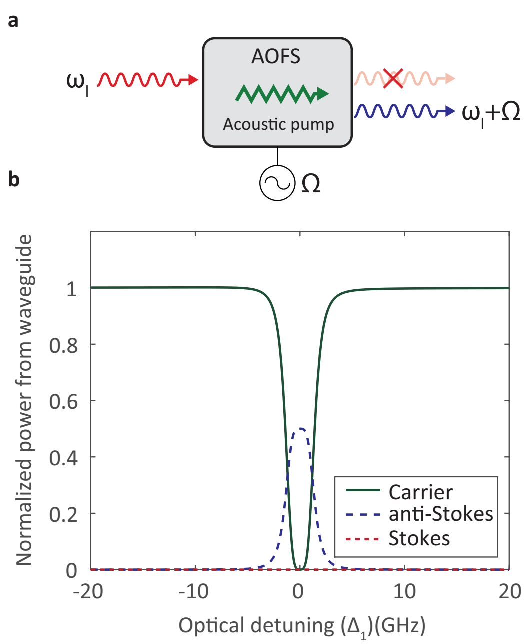

Figure S6: (a) Conceptual schematic of AOFS. (b) Example AOFS simulated based on the non-reciprocal modulator model. The carrier transmission is suppressed on resonance. 50% of power is converted into the anti-Stokes sideband.

Let us consider the transmission spectrum of TE_{10} mode ($\Delta_1 << \omega_2 - \omega_1$) in the forward phase matched case. We assume that the two optical modes are fully resolved ($\omega_2 - \omega_1 > \kappa_1/2$ and $\kappa_1/2$). The output from the waveguide can be expressed as:

$$|s_{out}|^2 = |s_{in} - \sqrt{\kappa_{ex1}}\, a_{1,0} + \sqrt{\kappa_{ex2}}\, a_{2,+1} e^{-i\Omega t}|^2 \tag{S33}$$

From Eq. S7a, we find that the transmission of the carrier laser vanishes ($s_{in} - \sqrt{\kappa_{ex1}}\, a_{1,0} = 0$), when the following equation is satisfied.

$$|G_{ph}|^2 = \frac{\kappa_2}{2}\left(\kappa_{ex1} - \frac{\kappa_1}{2}\right) \tag{S34}$$

Therefore, the output from the waveguide is only an anti-Stokes sideband, which can be represented as:

$$|s_{out}|^2 = \left| \frac{-iG_{ph}\sqrt{\kappa_{ex1}\kappa_{ex2}}}{(\kappa_2/2 - i(\Delta_2 + \Omega))(\kappa_1/2 - i\Delta_1) + |G_{ph}|^2} s_{in} e^{-i\Omega t} \right|^2 \tag{S35}$$

From Eq. S34, we see that the carrier transmission can be fully suppressed for certain optomechanical coupling coefficient (G_{ph}) such that the resonator is over-coupled to the waveguide ($\kappa_{ex1} > \kappa_1/2$). In other words, when the combined photon loss rate induced by the scattering process and the intrinsic loss is the same as the external coupling rate, the optical mode is critically coupled to the waveguide. Based on the above equations, we calculate output spectrum of the TE_{10} mode from the waveguide (Fig. S6b). In this simulation, we assume that $\kappa_{ex1} = \kappa_{ex2} = 1.5$ GHz and $\kappa_1 = \kappa_2 = 2$ GHz. As shown in Figure S7, when the acoustic power satisfying Eq. S34 is applied to the system, the carrier is fully absorbed by the resonator and only the anti-Stokes light comes out from the waveguide.

S7 Racetrack Resonator Dimensions

Specific geometry of our racetrack device is shown in Fig. S7. The resonator is composed of a 2.2 μm width waveguide, having 170 μm linear regions and 100 μm radius curved regions. Thus, the total circumference of the racetrack resonator is 968 μm. The resonator is fabricated on 350 nm of AlN on silicon substrate, which is undercut to confine light and the S_0 Lamb acoustic wave in AlN only. The ridge for the racetrack is defined by 200 nm deep etches on either side. This leaves behind 150 nm of AlN such that the racetrack is mechanically supported by the rest of the substrate and is acoustically linked to it.

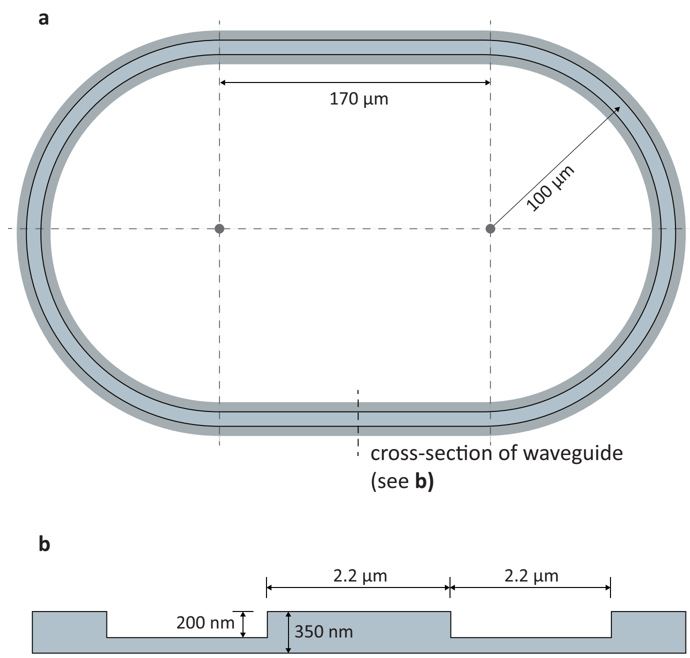

Figure S7: Dimensions of the racetrack optical resonator produced in this work that supports the required two optical modes.

S8 Tabular Summary of Device Parameters

Table S1: Summary of the device parameters.

	Parameters	Unit	†Mode pair 1	†Mode pair 2	†Mode pair 3
Two-mode Optical Racetrack Resonator	Frequency separation of TE_{10} and TE_{00} modes ($\omega_1 - \omega_2$)	GHz	4.55	8.01	-11.76
	Total loss rate of TE_{10} mode (κ_1)	GHz	2.04	2.46	2.66
	Total loss rate of TE_{00} mode (κ_2)	GHz	1.14	1.00	0.76
	Quality factor of TE_{10} mode (Q_1)	-	9.54×10^4	7.91×10^4	7.32×10^4
	Quality factor of TE_{00} mode (Q_2)	-	1.71×10^5	1.95×10^5	2.56×10^5
	External coupling rate (κ_{ex1})	GHz	0.74	0.85	0.8
	External coupling rate (κ_{ex2})	GHz	0.39	0.41	0.11
	*Wave number difference ($k_2 - k_1$)	m^{-1}		3.54×10^5	
S_0 Lamb Acoustic Wave	Transverse wave number ($q_{transverse}$)	m^{-1}		2.86×10^6	
	Propagating wave number ($q_{propagating}$)	m^{-1}		3.54×10^5	
	Total wave number (q_{total})	m^{-1}		2.88×10^6	
	IDT Pitch (Λ)	μm		2.186	
	IDT Aperture (W)	μm		123.00	
	IDT Angle (θ)	$^\circ$		7.06	
	Center frequency (Ω_m)	GHz		4.82	
	Driving frequency (Ω)	GHz		4.82	
	Bandwidth (Γ)	MHz		56	
	Acutation efficiency (η_a)	-		3.9%	
	*Acoustic proportionality factor in Eqn. S31 (γ)	J/m^3		2.55×10^{11}	
Acoustic-optic Interaction	Phonon enhanced optomechanical coupling (G_{ph})	GHz	0.066	0.073	0.024
	Optomechanical coupling (β)	GHz/nm	1.64	1.81	0.60

*From FEM simulation † Mode pairs are identified in the main manuscript

References

[1] Agarwal, G. S. & Jha, S. S. Multimode phonon cooling via three-wave parametric interactions with optical fields. *Phys. Rev. A* **88**, 013815 (2013).

[2] Bowen, W. P. & Milburn, G. J. *Quantum optomechanics* (CRC Press, 2015).

[3] Bochmann, J., Vainsencher, A., Awschalom, D. D. & Cleland, A. N. Nanomechanical coupling between microwave and optical photons. *Nat. Phys* **9**, 712–716 (2013).

[4] Li, H., Tadesse, S. A., Liu, Q. & Li, M. Nanophotonic cavity optomechanics with propagating acoustic waves at frequencies up to 12 GHz. *Optica* **2**, 826–831 (2015).